2017 21st International Conference on Process Control (PC)
June 6–9, 2017, Štrbské Pleso, Slovakia

Modeling of magnetic levitation system

Peter Balko, Danica Rosinová
Institute of Automotive Mechatronics
Slovak University of Technology in Bratislava
Bratislava, Slovakia
danica.rosinova@stuba.sk, peter.balko@stuba.sk

***Abstract*—The paper is devoted to modeling and parameter identification for Magnetic Levitation System (MLS) from Inteco. MLS belongs to challenging modelling and control problems due to its unstability and nonlinearity. We concern several modeling details not sufficiently described in user manual, a correction of nonlinear model, and present the corresponding measurement results. The obtained nonlinear model parameters and corresponding linearized model fits the real data much better than parameters provided in the reference.**

Keywords—nonlinear system, modeling, unstable system, magnetic levitation (maglev)

I. INTRODUCTION

Magnetic levitation belongs to well-known type of systems with variety of application field, [1]-[4]. Modeling the magnetic levitation system belongs to challenging tasks, since besides nonlinearities we have to cope with open-loop unstable system with fast dynamics and very small degree of natural damping. The basic control aim is to precisely position the levitating object, which requires adequately precise model. There exist many references devoted to modelling and control of various types of magnetic levitation laboratory plants, [5]-[8], to list a few. The laboratory MLS provided by Inteco is analyzed e.g. in [9], [11], [12], however, to the authors best knowledge, several important modeling details have not been sufficiently reported.

Basically, a mathematical model can be obtained from basic physical laws (first principles) or by data driven identification methods based on measurement of input and output data for adequately excited system, [10]. Frequently, both these approaches are combined, the structure is determined according to a theoretical (first principle based) model and parameter values are estimated from measured data using identification methods.

In this paper, we present our results on modeling the laboratory magnetic levitation system [7] with 2 electromagnets. The controlled output is a ball position between the electromagnets, where we consider only the upper one.

We present a model based on first principles, with simplified nonlinearities, where the respective parameters are estimated from measured data and verified by simulations and the resulting model is compared with experimental results on real laboratory plant.

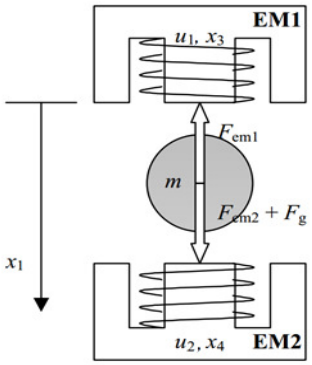

Fig. 1. Magnetic Levitation System with 2 Electromagnets EM1 and EM2 and a levitating sphere ball between them.

II. MAGNETIC LEVITATION SYSTEMS: PHYSICAL MODEL

Magnetic levitation can be briefly characterized as achieving the equilibrium of an object in the air-space without contact with solid substance, by using electromagnetic forces. In MLS, Fig. 1, a ferromagnetic object (a ball) is kept in the air-space between two electromagnets, where the upper one provides a vertical force overcoming the ball gravity and the lower one is used as additional, mainly for stabilization of a ball horizontal position.

A. Development of a Magnetic levitation model

The nonlinear physical model of the MLS can be described by state equations obtained from basic physical laws for a ball (sphere) motion in electromagnetic field, [9], [11].

Description of a ball dynamics and of electromagnetic forces is based on Lagrange function - the difference between kinetic and potential energy, which can be written as

$$T = \frac{1}{2}m\dot{x}^2 + \frac{1}{2}L(x)\dot{q}^2 + \frac{1}{2}\int_0^t R\dot{q}^2 dt + mgx + qu \qquad (1)$$

where x is a distance of the sphere from electromagnet, q is electric charge, m is a mass of the sphere, R is a resistance of the electromagnet coil, $L(x)$ is a function describing the

dependence of inductance of the coil on distance x, $I = \dot{q}$ is a current in the coil, g is gravity constant, u is voltage.

Variables $x(t), q(t)$ must meet the Lagrange equations

$$\begin{aligned} \frac{d}{dt}\frac{dT}{d\dot{x}} - \frac{\partial T}{\partial x} = 0 \\ \frac{d}{dt}\frac{dT}{d\dot{q}} - \frac{\partial T}{\partial q} = 0 \end{aligned} \tag{2}$$

which yield

$$\begin{aligned} \frac{d^2x}{dt^2} &= \frac{1}{2m}\frac{dL}{dx}I^2 + g, \\ \frac{dI}{dt} &= \frac{1}{L}\left(-\frac{dL}{dx}\frac{dx}{dt}I - RI + u\right) \end{aligned} \tag{3}$$

The first equation from (3) corresponds to Newton's second law, where an electromagnetic force is given by

$$F(x,I) = \frac{1}{2}\frac{dL}{dx}I^2 . \tag{4}$$

Dependence of coil inductance on distance can be approximated by polynomial or exponential functions

$$L(x) = L_0 + L_1 e^{-ax}, a > 0 \tag{5a}$$

$$\begin{aligned} &L(x) = L_0 + \frac{1}{a_n x^n + a_{n-1}x^{n-1} + ... + a^1 x_1 + a_0}, \\ &n \geq 1, a_0, ..., a_n \in R \end{aligned} \tag{5b}$$

Below, we will use the exponential alternative (5a), having

$$\frac{dL}{dx} = -aL_1 e^{-ax} \tag{6}$$

The second equation from (3) is simplified by the experimentally received approximation, [9]

$$\frac{dI}{dt} = -\frac{1}{f(x)}(ku + c - I) \tag{7}$$

where function $f(x)$ has a structure similar to (6). Introducing state variables

$x_1(t) = x(t) \approx$ position of the sphere,
$x_2(t) = \dot{x}_1(t) \approx$ velocity of the sphere,
$x_3(t) = I(t) \approx$ current in the upper coil,

and combining (3) and (7), the resulting nonlinear mathematical model is obtained, see [5,9]

$$\begin{aligned} \frac{dx_1}{dt} &= x_2, \\ \frac{dx_2}{dt} &= \frac{1}{2m}\frac{dL(x_1)}{dx_1}x_3^2 + g \\ \frac{dx_3}{dt} &= -\frac{1}{f(x_1)}(ku + c - x_3) \end{aligned} \tag{8}$$

Applying the approximation (6) with slightly different denotation, finally we obtain

$$\begin{aligned} \frac{dx_1}{dt} &= x_2, \\ \frac{dx_2}{dt} &= -\frac{F_{em1}}{2m} + g \\ \frac{dx_3}{dt} &= \frac{1}{f_i(x_1)}(k_i u + c_i - x_3) \end{aligned} \tag{9}$$

where

$$\begin{aligned} F_{em1} &= x_3^2 \frac{F_{emP1}}{F_{emP2}} \exp\left(-\frac{x_1}{F_{emP2}}\right), \\ f_i(x_1) &= \frac{f_{iP1}}{f_{iP2}} \exp\left(-\frac{x_1}{f_{iP2}}\right). \end{aligned}$$

Correspondence of the second equalities from (8) and (9) is through approximation (6) with

$$a \approx \frac{1}{F_{emP2}}, L_1 \approx F_{emP1}, \frac{dL}{dx} \approx -\frac{F_{emP1}}{F_{emP2}} \exp\left(-\frac{x_1}{F_{emP2}}\right).$$

The real laboratory model uses variables in the intervals

$$x_1 \in \langle 0, 0.016 \rangle, x_2 \in R, x_3 \in \langle i_{\min}, 2.38 \rangle, u \in \langle u_{\min}, 1 \rangle .$$

Remark 1: It should be noted that the second equation in nonlinear model (9) differs from the one presented in MLS documentation, [5]: there is coefficient 2 in the denominator corresponding to the first equation from (3). This coefficient appears then also in the linearized model below (in elements $a_{2,1}$ and $a_{2,3}$ in (13)).

B. Validation of model coefficients

This section presents validation of the key coefficients from nonlinear model (9) by measurements on laboratory plant. Since the plant itself is unstable, measurements are realized in closed-loop with stabilizing PD controller delivered by producer, [5].

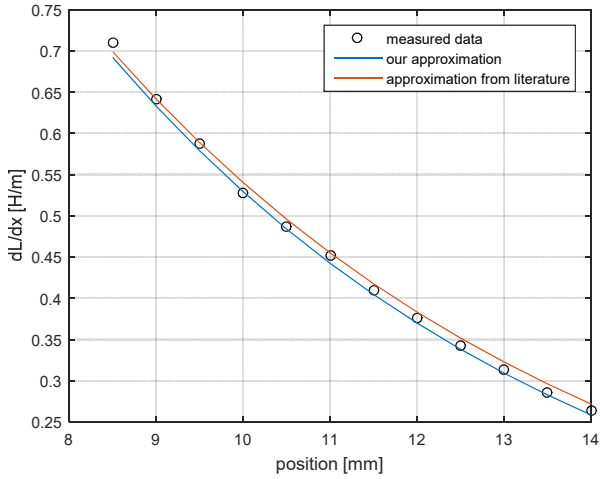

Fig. 2. Validation of approximation coefficients, obtained from measured dependence of coil current I on ball position x.

Coefficients F_{emP1} and F_{emP2} for approximation of dL/dx corresponding to (6), can be obtained by measuring the dependence of coil current x_3 on ball position x_1 in steady state. dL/dx is then computed from the second equality from (8)

$$0 = \frac{1}{2m}\frac{dL(x_1)}{dx_1}x_3^2 + g$$
$$\frac{dL(x_1)}{dx_1} = -g\frac{2m}{x_3^2} \qquad (10)$$

Measured data x_1, x_3 and u are given in Tab.I. The corresponding Fig.2 shows comparison of approximation for coefficients F_{emP1} and F_{emP2} obtained from measured data, and the coefficients reported in Inteco manual. We can confirm near accordance of measured and reported approximation coefficients.

TABLE I. MEASURED x_1, x_3 AND u FOR dL/dx_1 APPROXIMATION

Position (x_1) [mm]	Current (x_3) [A]	Control output (u) [MU]	$-dL/dx_1$ [H/m]
8.5	1.025	0.315	0.7096
9	1.078	0.328	0.6416
9.5	1.126	0.344	0.588
10	1.189	0.352	0.5274
10.5	1.237	0.362	0.4872
11	1.285	0.378	0.4515
11.5	1.35	0.392	0.4091
12	1.408	0.413	0.3761
12.5	1.475	0.423	0.3427
13	1.543	0.432	0.3131
13.5	1.617	0.446	0.2851
14	1.679	0.462	0.2645

All parameters of the above equations are given in Table II.

TABLE II. PARAMETERS OF THE EQUATIONS (1)

Parameters	Values	Units
m	0.016, 0.023, 0.039	kg
g	9.81	m/s^2
Fem1,Fem2	function of x1 and x3	N
FemP1	0.017521	H
FemP2	0.0058231	m
fi(x1)	function of x1	s^{-1}
fiP1	1.4142 10-4	ms
fiP2	4.5626 10-3	m
ci	-0.4	A
ki	4.4	A
xd	distance between electromagnets minus ball diameter (0.1- 0.033 / 0.04 / 0.054)	m
iMIN	0.03884	A
uMIN	0.00498	MU

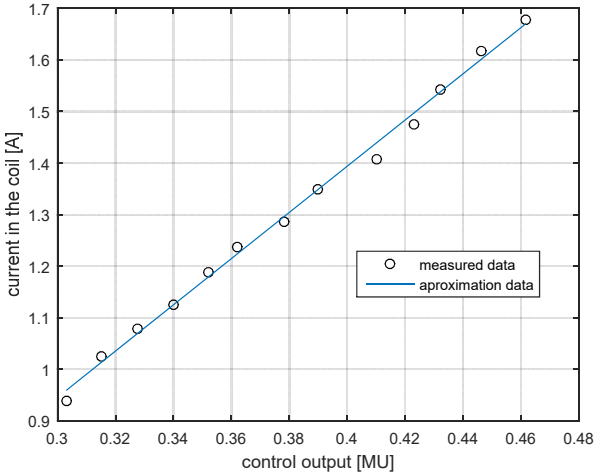

Fig. 3. Dependence of current x_3 on control output (provided in machine units) for all three balls

Parameters k_i and c_i are given by approximation of real measured data, see Fig.3. We made more experiments for all three balls, the average parameter values are

$$I = k_i u + c_i = 4.4u - 0.4. \qquad (11)$$

The difference between real data and approximation is very small, thus we can consider the corresponding nonlinear model as appropriate for linearization around equilibrium points. In this case, the obtained parameters k_i and c_i are significantly different from those reported in documentation, [5].

III. LINEARISATION OF MAGNETIC LEVITATION SYSTEM

The linearized state space model for (1) can be obtained using Jacobian linearization around the determined working point as

$$\dot{x}(t) = Ax(t) + Bu(t) = \begin{bmatrix} 0 & 1 & 0 \\ a_{2,1} & 0 & a_{2,3} \\ 0 & 0 & a_{3,3} \end{bmatrix} x(t) + \begin{bmatrix} 0 \\ 0 \\ b_3 \end{bmatrix} u(t)$$
$$y(t) = Cx(t) = \begin{bmatrix} 1 & 0 & 0 \end{bmatrix} x(t) \qquad (12)$$

where the elements of the A and B matrices are for the working point defined by $[x_{10}, x_{20}, x_{30}]$, given as

$$a_{2,1} = \frac{x_{30}^2}{2m}\frac{F_{emP1}}{F_{emP2}^2}\exp\left(-\frac{x_{10}}{F_{emP2}}\right)$$
$$a_{2,3} = -\frac{x_{30}}{m}\frac{F_{emP1}}{F_{emP2}}\exp\left(-\frac{x_{10}}{F_{emP2}}\right) \quad (13)$$
$$a_{3,3} = -\frac{1}{f_i(x_{10})}$$
$$b_3 = k_i\frac{1}{f_i(x_{10})}$$

Note that $a_{3,1} = 0$ since $k_i u + c_i - x_3 = 0$ in any working point.

To convert state space model to transfer function, we use

$$\det(sI - A) = 0$$

$$\det(sI - A) = \begin{bmatrix} s & -1 & 0 \\ -a_{2,1} & s & a_{2,3} \\ 0 & 0 & s + a_{3,3} \end{bmatrix} \quad (14)$$

$$\det(sI - A) = \left(s^2 - a_{2,1}\right)\left(s + a_{3,3}\right) = \left(s - \sqrt{a_{2,1}}\right)\left(s + \sqrt{a_{2,1}}\right)\left(s + a_{3,3}\right)$$

The resulting transfer function is

$$G(s) = \frac{Y(s)}{U(s)} = C^T(sI - A)^{-1}B = \frac{-b_3 a_{2,3}}{\left(s^2 - a_{2,1}\right)\left(s + a_{3,3}\right)} \quad (15)$$

The input current respective to the position of the ball is depicted in Fig. 4 for all three balls. This dependence is used for determining the working point corresponding to the required ball position.

In the following we present three linearized models, where parameters m, x_{30}, u_0 vary for big, medium and small balls.

Determination of the working point

The working point is determined by a required ball position x_{10}. Thus the working point is set by the next steps.

i) choose the ball size m and its position x_{10};

ii) set the value of x_{30} corresponding to the determined x_{10} (see Fig.4.), alternatively – calculate x_{30} from the second equation from (9) in steady state for $x_1 = x_{10}$;

iii) calculate u_0 for the determined x_{10} and x_{30} from (11): $x_{30} = k_i u_0 + c_i = 4.4u_0 - 0.4$.

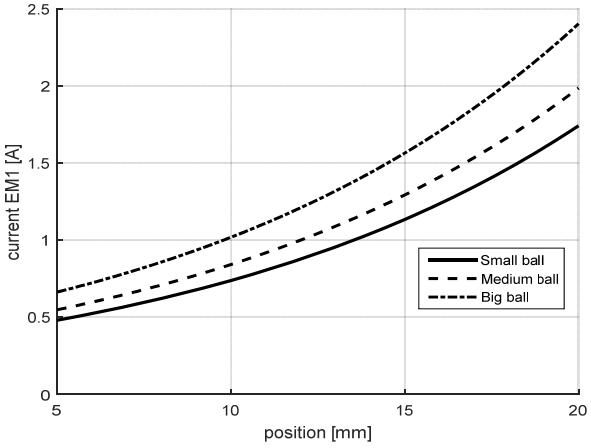

Fig. 4. Dependence of coil current on ball position

Big ball linearized model

We consider the working point $x_{10} = 0.01[m]$, $x_{30} = 1.19[A]$ and $u_{10} = 0.363[MU]$, the state space model is

$$\dot{x}(t) = Ax(t) + Bu(t) = \begin{bmatrix} 0 & 1 & 0 \\ 1685 & 0 & -16.5 \\ 0 & 0 & -288.8 \end{bmatrix}x(t) + \begin{bmatrix} 0 \\ 0 \\ 1271 \end{bmatrix}u(t)$$
$$y(t) = Cx(t) = \begin{bmatrix} 1 & 0 & 0 \end{bmatrix}x(t)$$

and the respective transfer function is

$$G_1(s) = \frac{-20947}{(s + 288.8)(s + 41.04)(s - 41.04)}. \quad (16)$$

Medium ball linearized model

We consider the working point $x_{10} = 0.01[m]$, $x_{30} = 0.914[A]$ and $u_{10} = 0.300[MU]$, the state space model is

$$\dot{x}(t) = Ax(t) + Bu(t) = \begin{bmatrix} 0 & 1 & 0 \\ 1685 & 0 & -21.5 \\ 0 & 0 & -288.8 \end{bmatrix}x(t) + \begin{bmatrix} 0 \\ 0 \\ 1271 \end{bmatrix}u(t)$$
$$y(t) = Cx(t) = \begin{bmatrix} 1 & 0 & 0 \end{bmatrix}x(t)$$

and the respective transfer function is

$$G_2(s) = \frac{-27277}{(s + 288.8)(s + 41.04)(s - 41.04)}. \quad (17)$$

Small ball linearized model

We consider the working point $x_{10} = 0.01[m]$, $x_{30} = 0.762[A]$ and $u_{10} = 0.265[MU]$

$$\dot{x}(t) = Ax(t) + Bu(t) = \begin{bmatrix} 0 & 1 & 0 \\ 1685 & 0 & -25.7 \\ 0 & 0 & -288.8 \end{bmatrix} x(t) + \begin{bmatrix} 0 \\ 0 \\ 1271 \end{bmatrix} u(t)$$
$$y(t) = Cx(t) = \begin{bmatrix} 1 & 0 & 0 \end{bmatrix} x(t)$$

and the respective transfer function is

$$G_3(s) = \frac{-32704}{(s+288.8)(s+41.04)(s-41.04)}. \qquad (18)$$

Note that only gain varies with the ball change.

Comparison between real and linearised system

In this section, step responses around working points for all three balls are shown for:

1) real laboratory MLS;

2) nonlinear model (9) with parameter values given in Tab.II, denoted as nonlin. model 1;

3) nonlinear model with parameters from [5], denoted as nonlin. model 2;

4) linearized models (16), (17) and (18) for big, medium and small ball respectively.

The MLS system is unstable. Therefore the comparison is realized in closed loop with stabilizing controller. In our case, we use a PID controller corresponding to (20) with parameters

P=125; I=377 830; D=5.65.

(Note that sampling time for MLS is 1ms.)

The results are illustrated in the next pictures. Comparison shows that the developed nonlin. model 1 as well as the corresponding linearized model better fits the real MLS response than nonlin. model 2 reported in [5]. (Reason can be in slightly different parameters of the individual MLSs.)

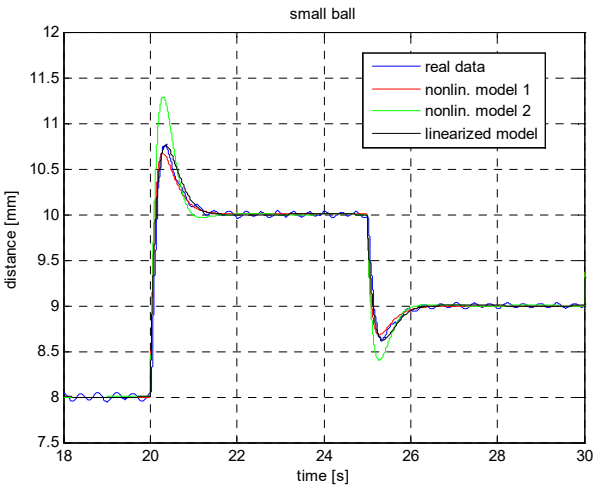

Fig. 5. Comparison of the output responses of the developed model, linearized one, nonlinear model from [5] and real measured data for small ball

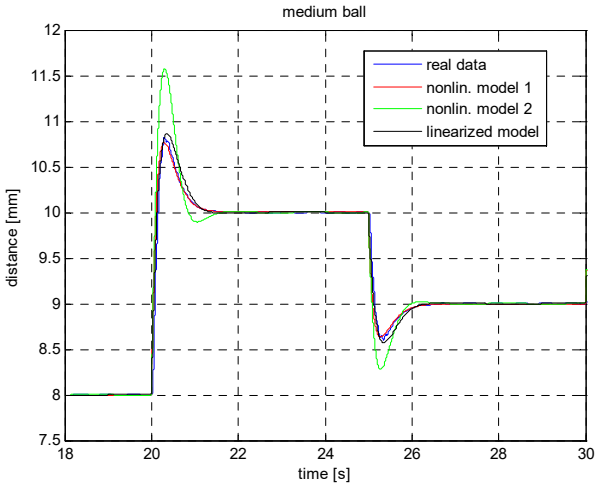

Fig. 6. Comparison of the output responses of the developed model, linearized one, nonlinear model from [5] and real measured data for medium ball

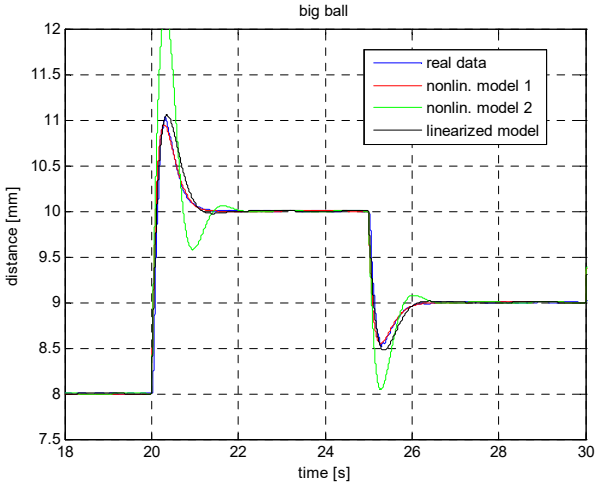

Fig. 7. Comparison of the output responses of the developed model, linearized one, nonlinear model from [5] and real measured data for big ball

It is important to note that though thesystem is highly nonlinear, the linearized model works well around the working point.

IV. Stability Conditions for a Closed Loop with PID Controller

In this section, necessary stability conditions are developed for the closed loop comprising linearized MLS model with PID controller, which indicates the required controller structure and parameters.

Due to negative gain of the MLS transfer function (16), (17), (18), positive feedback is considered to obtain control error. The PID controller design is then based on closed loop

$$G_{CL}(s) = \frac{G_{PID}(s)G(s)}{1 - G_{PID}(s)G(s)} \tag{19}$$

where $G(s)$ correspond to MLS transfer function (15), its parameters are determined by working point and respective ball (see (16), (17), (18)); $G_{PID}(s)$ is transfer function of PID controller in the form

$$G_{PID}(s) = P + \frac{I}{s} + Ds\,. \tag{20}$$

Closed-loop characteristic polynomial for (19) with $G(s)$ and $G_{PID}(s)$ given by (15) and (20) is

$$CHP = s^4 - a_{3,3}s^3 - (a_{2,1} + b_3 a_{2,3})s^2 + (a_{2,1}a_{3,3} - b_3 a_{2,3}P) - b_3 a_{2,3}I \tag{21}$$

Recall the parameter signs (compare (15) with e.g. (16))

$a_{2,1} > 0;\ \ a_{2,3} < 0; a_{3,3} < 0;\ \ b_3 < 0$, therefore

$a_{2,1}a_{3,3} < 0;\qquad b_3 a_{2,3} > 0$

Applying Routh stability criterion on (21) we receive closed loop stability conditions

$$D > \frac{a_{2,1}}{-b_3 a_{2,3}};\qquad P > \frac{a_{2,1}a_{3,3}}{b_3 a_{2,3}} \tag{22}$$

Therefore

$$D > -\frac{P}{a_{3,3}}\,. \tag{23}$$

Stability analysis shows that minimal stabilizing structure comprises proportional P and derivative D term. To avoid steady-state error, integral term is required as well.

Controller design procedure is not included in this paper, one possible control design procedure is described in [14].

V. Conclusion

We have presented several details on modelling Magnetic levitation system delivered by Inteco, not reported in the system documentation, and corrected a mistake in theoretical model. The experiments to verify values of model parameters are described in details; the respective results show the major difference in linear approximation of dependence of coil current on input voltage in comparison with [5]. Modifying the model parameter values according to measured data provides nonlinear and respective linearized model with step response very close to the real experiments.

Acknowledgment

The work has been supported by the SRDA grant No APVV 0772-12 and Slovak Scientific Grant Agency, grant No 1/0733/16.

References

[1] P. Holmer, “Faster than a speeding bullet train”, IEEE Spectrum, Vol. 40, No. 8, 2003, pp. 30-34.

[2] M. Varvella, E. Calloni, L. Di Fiore, L. Milano, N. Arnaud, “Feasibility of magnetic suspension for second generation gravitational wave interferometers”, Astroparticle Physics, Vol. 21, No. 3, 2004, pp. 325-335.

[3] P.J. Berkelman, R.L. Hollis, “Lorentz magnetic levitation for haptic interaction: Device design, performance, and integration with physical simulations”, International Journal of Robotics Research, Vol. 19, No. 7, 2000, pp. 644-667.

[4] M.B. Khamesee, N. Kato, Y. Nomura, T. Nakamura, “Design and control of a microrobotic system using magnetic levitation”, EEE-ASME Transactions on Mechatronics, Vol. 7, No. 1, 2002, pp. 1-14.

[5] Magnetic Levitation System 2EM – User’s Manual (Inteco Ltd, Krakow, Poland, 2008).

[6] Magnetic Levitation Experiment, Quanser Consulting Inc.

[7] CE 152 Magnetic Levitation Model, Humusoft, http://www.humusoft.cz/models/ce152/

[8] MA 401 Laboratory Setup Magnetic Suspension, Amira.

[9] P. Bania, “Model I sterowanie magnetyczna lewitacja”, Diploma thesis, University of Science and Technology (AGH) in Krakow, 1999

[10] L. Sun, Y. Miyake, H. Ohmori, A. Sano, “New Direct Closed-Loop Identification Method for Unstable Systems and Its Application to Magnetic Suspension System”, Trans. of the Society of Instrument and Control Engineers, Vol. E-2 (2002), No.1, pp.72-80.

[11] A. Turnau, K. Kolek, “Time-optimal and PID variable structure controller”. Proceedings of the Mediterranean Conference on Electronics and Automatic Control MCEA’98, Marrakech, 17-19 September, Maroc, 1998, pp. 476-479.

[12] R. C. David, C. A. Dragoş, R. G. Bulzan, R. E. Precup, E. M. Petriu, M. B. Rădac, „An approach to fuzzy modeling of magnetic levitation systems“, International Journal of Artificial Intelligence, vol. 9, no. A12, 2012, pp. 1-18.

[13] C. J. Munaro, M. R. Filho, R. M. Borges, S. da Silva Munareto, W.T. da Costa, „Modeling and observer-based nonlinear control of a magnetic levitation system“, in Proceedings of the 2002 IEEE International Conference on Control Applications, 2002, pp.162-167

[14] M. Hypiusova, A. Kozakova, „Robust PID controller design for magnetic levitation system – Frequency domain approach, submitted to 21st International Conference on Process Control, Štrbské Pleso, Slovakia, June 2017.